Electronic Supplementary Information

Three polymorphs of one luminogen: How the molecular packing affects the RTP and AIE properties?

Jie Yang, Zichun Ren, Bin Chen, Manman Fang, Zujin Zhao, Ben Zhong Tang, Qian Peng and Zhen Li*

Contents

calculations at the b3lyp/6-31g* level.

Table S3 The excitation energy, oscillator strength and orbital assignment of CzS-CN in the first three excited singlet states evaluated by the TD-DFT (b3lyp/6-31g*) calculation.

Table S4 The energy levels and gaps between S_1 and T_1 states for the isolated and coupled units in three polymorphs from the TD-DFT calculation.

Figure S12 The general diagram for the PL process.

Figure S13 The molecular structures and the respective energy gaps between S_1 and T_1 states for the isolated and coupled units in three polymorphs.

Figure S14 The molecular configurations and the respective transition dipole moments (blue arrows) from S_0 to S_1 states for the three polymorphs.

Figure S15 Splitting of the optically allowed transitions of X-type coupled units, isolated molecule and H-type coupled units (upper); the images of the three polymorphs under UV-irradiation taken by optic microscope Leica M123 (down).

Figure S16 Examples for some polymorphs with diverse emissive properties

Figure S17 The molecular structure, mechanoluminescence (ML) phenomenon and the crystal analyses of polymorphs for P_4TA—the different molecular configurations with different dipole moments, led to the different ML property.

Figure S18 The molecular structure, PL emissive pictures and the crystal analyses of polymorphs for TDHA—the different molecular configurations with different torsion angles, led to the different PL emissions.

Figure S19 The molecular structure, mechanoluminescence (ML) phenomenon and the crystal analyses of polymorphs for TMPE—the different packing modes with different intermolecular interactions, led to the different ML property.

Figure S20 The molecular structure, mechanoluminescence (ML) phenomenon and the crystal analyses of polymorphs for C2—the different packing modes with excimer or not, led to the different PL emissions.

1. General Information

Characterization

^{1}H NMR and ^{13}C NMR spectra were recorded on a 400 MHz Bruker Ascend spectrometer using $CDCl_3$ as solvent. Mass spectra were conducted on a ZAB 3F-HF mass spectrophotometer. Elemental analyses of carbon, hydrogen, nitrogen and sulfur were measured on a Perkin-Elmer microanalyzer. UV-vis spectra were performed on a Shimadzu UV-2550. Photoluminescence spectra at room temperature and 77K were performed on a Hitachi F-4600 fluorescence spectrophotometer. Photoluminescence quantum yields were determined with a HamamatsuC11347 Quantaurus-QY absolute quantum yield spectrometer. Fluorescence lifetimes were determined with a Hamamatsu C11367-11 Quantaurus-Tau time-resolved spectrometer. The powder X-ray diffraction patterns were recorded by Bruker D8 Advance at a scan rate of 8^{o} (2θ)/min (scan range: 5-50^{o}). The single-crystal X-ray diffraction data were collected in a Bruker APEX-II CCD diffractometer.

The Gaussian 09 program was utilized to perform the TD-DFT calculations. The ground state (S_0) geometries were obtained from the single crystal structures and no further geometry optimization was conducted in order to maintain the specific molecular configurations. The vertical excitation energies of the *n*-th singlet (S_n) and *n*-th triplet states (T_n) were obtained on the corresponding ground state structures using the TD-b3lyp/6-31g*. The transition dipole moments were calculated through the same method. Kohn-Sham frontier orbital analyses and spin density distributions were obtained in order to elucidate the mechanisms of possible singlet-triplet intersystem crossings (ISC).

Synthesis

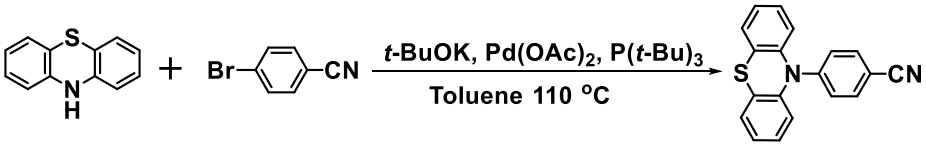

Scheme S1 The synthetic route of CzS-CN.

CzS-CN: Phenothiazine (1.99 g, 10 mmol), 4-Bromobenzonitrile (1.82 g, 10 mol), potassium tert-butoxide (1.68 g, 15 mmol), palladium acetate (0.11 g, 0.5 mmol) and tri-tert-butylphosphine solution (0.5 mL, 0.25 mmol) were dissolved in toluene (100 mL) in a Schlenk tube. The resultant mixture was refluxed for 12 hours under argon, then extracted with dichloromethane. The combined organic extracts were dried over anhydrous Na_2SO_4 and concentrated by rotary evaporation. The crude product was purified by column chromatography on silica gel using petroleum ether/dichloromethane (3:1 v/v) as eluent to afford a white solid in a yield of 70%. ^{1}H-NMR (400 MHz, $CDCl_3$) δ (ppm): (ppm): 7.43-7.49 (m, 4H), 7.28-7.32 (m, 4H), 7.19-7.23 (m, 2H), 7.05-7.08 (m, 2H). ^{13}C-NMR (100 MHz, $CDCl_3$) δ (ppm): 148.9, 140.8, 133.5, 133.1, 128.9, 127.4, 127.3, 126.2, 126.0, 119.5, 116.5. MS (EI), m/z: 300.03 ([M^+], calcd for $C_{19}H_{12}N_2S$, 300.07. Anal. Calcd for $C_{19}H_{12}N_2S$: C, 75.97; H, 4.03; N, 9.33; S 10.67. Found: C, 76.21; H, 3.93; N, 9.29; S, 10.65.

Cultivation of single crystal

Needle-like crystal (A) was cultured from the dichloromethane, methanol and ethyl acetate mixture with respective fractions about 5: 4.5: 0.5; block-like crystal (B) was from pure dichloromethane solution while flake-like crystal (C) from the dichloromethane, hexane and methanol mixture with respective fractions about 5: 4.5: 0.5.

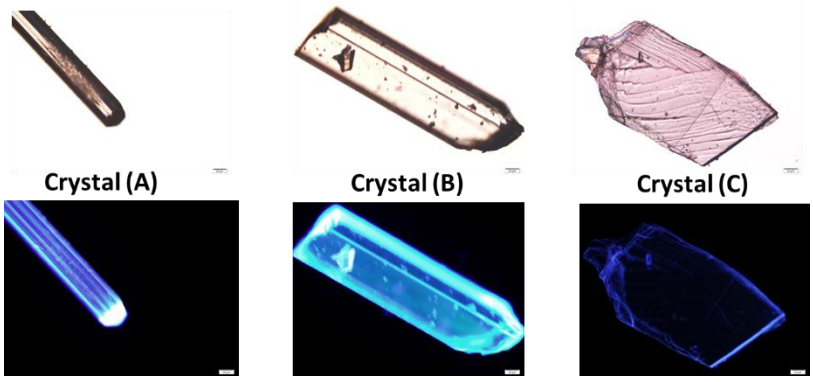

Figure S1 The pictures of the three polymorphs under daylight (upper) and UV-irradiation (down) taken by optic microscope Leica M123.

Table S1 The photophysical data of CzS-CN in different states.

Compound	State	Φ_{PL} (%)	λ_F (nm)	τ_F (ns)	λ_P (nm)	τ_P (ms)	α_{AEE}[a]
CzS-CN	THF	2.1	529	/	/	/	/
	Crystal A	22.6	410	1.32	521	226	10.8
	Crystal B	17.8	430	2.95	516	41	8.5
	Crystal C	6.9	380	0.94	539	32	3.3
	As prepared	20.9	430	3.09	508	43	10.0
	ground	23.6	497	/	503	11	11.2
	Fumed	27.2	440, 497	/	505	14	13.0

[a] These data were calculated through the formula $\alpha_{AEE} = \Phi_{solid,PL}/\Phi_{THF,PL}$

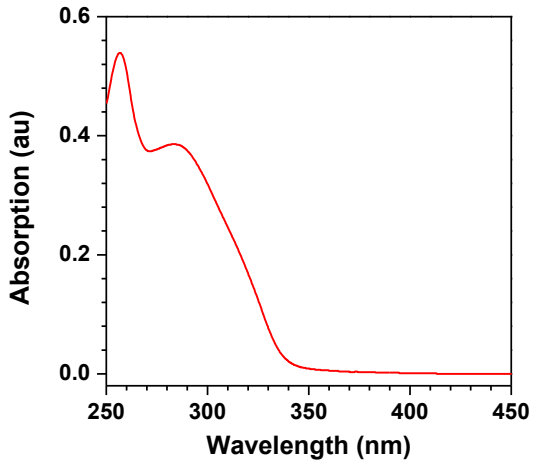

Figure S2 The UV-visible spectrum of the dilute THF solution for CzS-CN (concentration ≈ 10 μM).

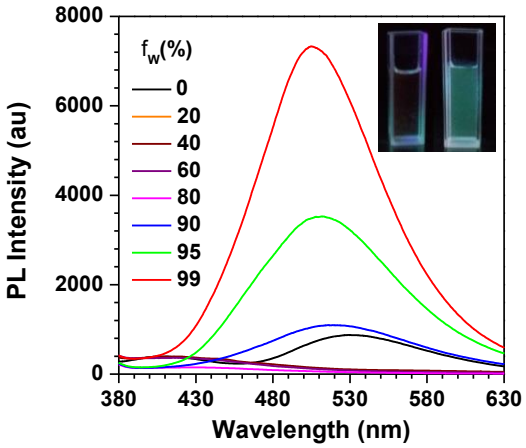

Figure S3 The PL spectra of CzS-CN in the mixtures of THF/water with different water fractions (concentration ≈ 10 μM).

Table S2 Structural data of CzS-CN for crystal (A), crystal (B) and crystal (C).

Name	Crystal (A)	Crystal (B)	Crystal (C)
Formula	$C_{19}H_{12}N_2S$	$C_{19}H_{12}N_2S$	$C_{19}H_{12}N_2S$
Wavelength (Å)	0.71073	0.71073	0.71073
Space Group	P 21/c	P-1	P 21/C
Cell Lengths (Å)	a=12.3262(17) b=12.5229(18) c=9.8675(14)	a=10.3472(10) b=12.6805(12) c=12.7346(12)	a=16.315(5) b=12.408(4) c=7.380(2)
Cell Angles (°)	α=90 β=107.314(2) γ=90	α=91.281(1) β=109.390(1) γ=111.059(1)	α=90.00 β=94.840 (5) γ=90.00
Cell Volume (Å^3)	1454.1(4)	1451.7(2)	1488.7 (8)
Z	4	4	4
Density (g/cm^3)	1.372	1.374	1.340
F(000)	624.0	624.0	624.0
CCDC Number	1555300	1555301	1555302

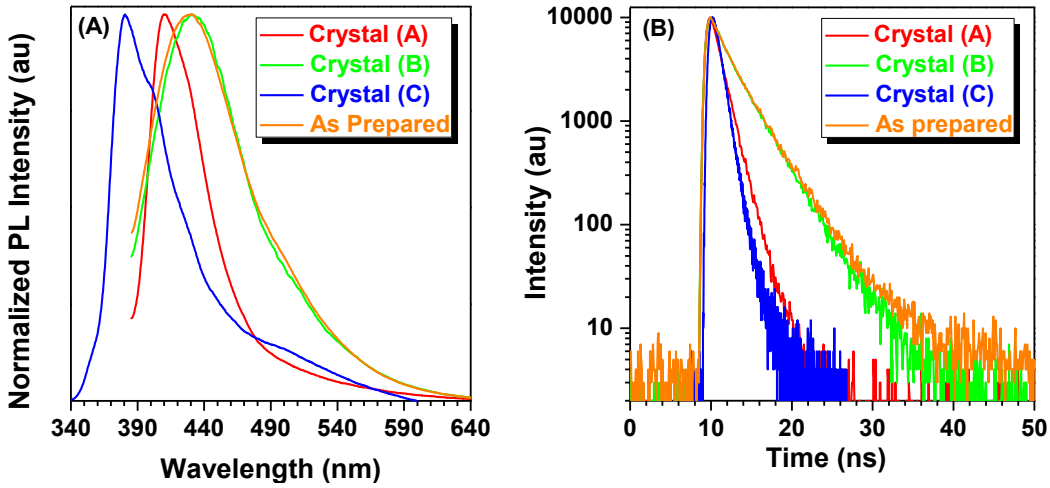

Figure S4 (A) The normalized PL spectra of CzS-CN in crystal (A), crystal (B), crystal (C) and as prepared powder; **(B)** The fluorescence decay of CzS-CN in crystal (A), crystal (B), crystal (C) and as prepared powder.

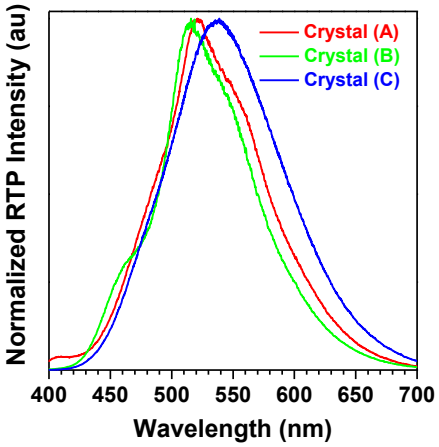

Figure S5 The normalized room temperature phosphorescence spectra of CzS-CN for crystal (A), crystal (B) and crystal (C).

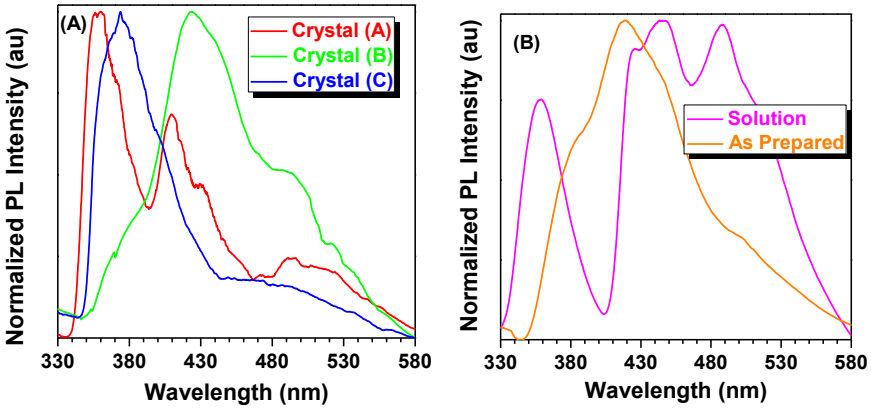

Figure S6 (A) The normalized PL emission spectra of CzS-CN for crystal (A), crystal (B) and crystal (C) at 77K; **(B)** The normalized PL emission spectra of CzS-CN for THF solution and as prepared powder at 77K.

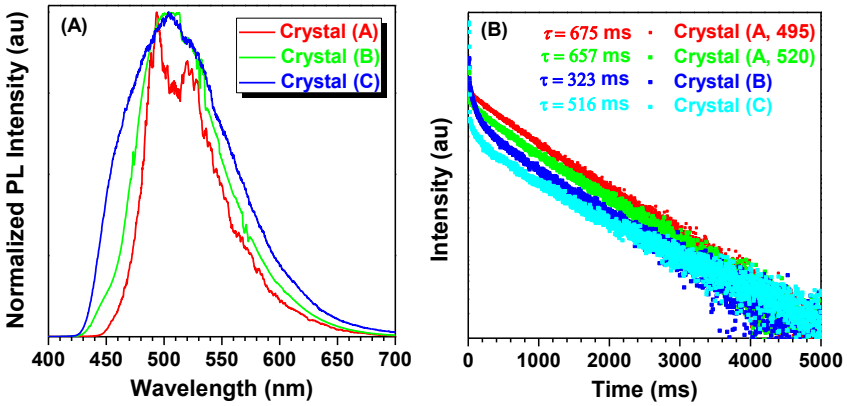

Figure S7 (A) The normalized phosphorescence spectra of CzS-CN for crystal (A), crystal (B) and crystal (C) at 77K; **(B)** The time-resolved PL-decay curves for phosphorescence at 77K in crystal (A), crystal (B) and crystal (C).

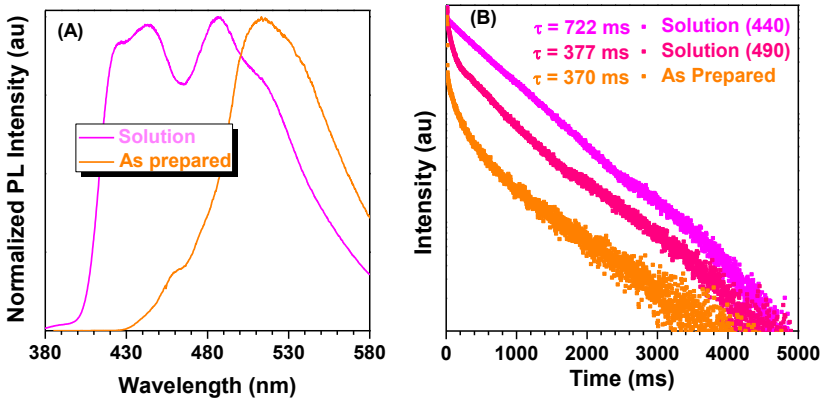

Figure S8 (A) The normalized phosphorescence spectra of CzS-CN for THF solution and as prepared powder at 77K; **(B)** The time-resolved PL-decay curves for phosphorescence at 77K in THF solution and as prepared powder.

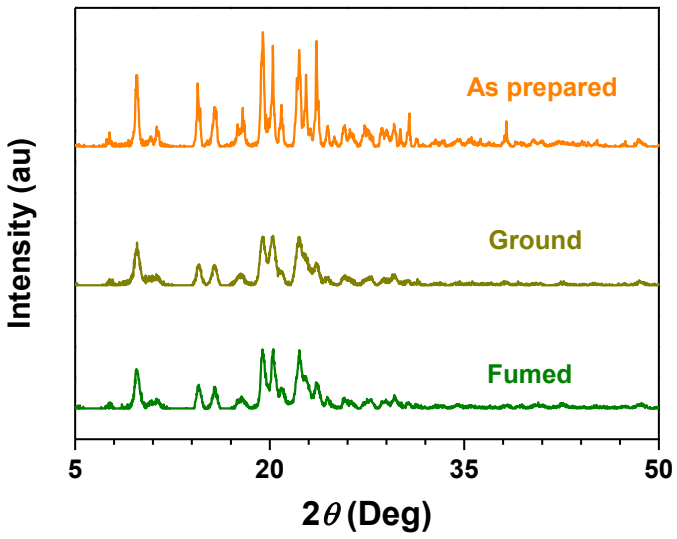

Figure S9 The PXRD patterns for CzS-CN in as prepared, ground and fumed powder.

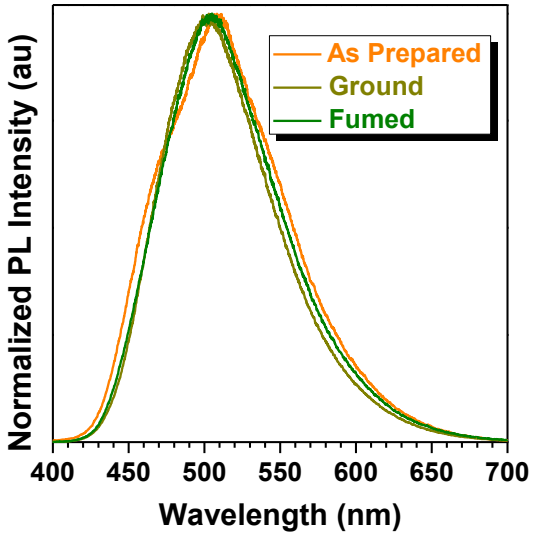

Figure S10 The normalized room temperature phosphorescence spectra for CzS-CN in as prepared, ground and fumed powder.

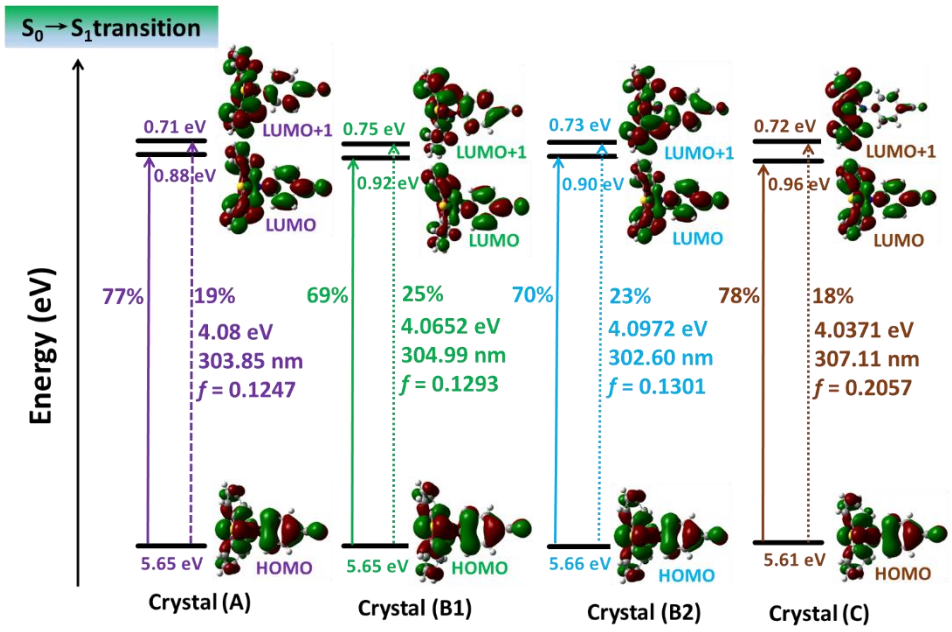

Figure S11 Energy diagrams and the frontier orbitals contributions of CzS-CN in different crystals and their energy transitions for S_0 to S_1 state estimated by TD-DFT calculations at the b3lyp/6-31g* level.

Table S3 The excitation energy, oscillator strength and orbital assignment of CzS-CN in the first three excited singlet states evaluated by the TD-DFT (b3lyp/6-31g*) calculation.

	transition	excitation energy	Absorption[nm] (oscillator strength)	Assignments
Crystal (A)	$S_0 \rightarrow S_1$	4.08 eV	303.85 (0.1247)	H→L (76.7%), H→L+1 (19.0%)
	$S_0 \rightarrow S_2$	4.19 eV	295.75 (0.0041)	H→L+1 (6.7%), H→L+2 (82.1%), H→L+3 (7.7%)
	$S_0 \rightarrow S_3$	4.30 eV	288.60 (0.0497)	H→L (4.2%), H→L+1 (26.7%) H→L+3 (61.9%)
Crystal (B_1)	$S_0 \rightarrow S_1$	4.07 eV	304.99 (0.1293)	H→L (68.6%), H→L+1 (25.3%) H→L+2 (2.8%)
	$S_0 \rightarrow S_2$	4.17 eV	297.01 (0.0112)	H→L (2.2%),H→L+1 (24.9%),H →L+2 (61.4%), H→L+3 (8.3%)
	$S_0 \rightarrow S_3$	4.28 eV	289.83 (0.0693)	H→L (7.3%), H→L+1 (22.2%), H →L+3 (65.1%)
Crystal (B_2)	$S_0 \rightarrow S_1$	4.10 eV	302.60 (0.1301)	H→L (69.9%), H→L+1 (23.2%), H→L+2 (3.0%)
	$S_0 \rightarrow S_2$	4.19 eV	296.05 (0.0057)	H→L+1 (9.9%), H→L+2 (77.4%), H→L+3 (9.8%)
	$S_0 \rightarrow S_3$	4.29 eV	289.06 (0.0803)	H→L (9.2%), H→L+1 (36.3%), H →L+3 (48.9%)
Crystal (C)	$S_0 \rightarrow S_1$	4.04 eV	307.11 (0.2057)	H→L (77.7%), H→L+1 (18.2%), H→L+4 (2.3%)
	$S_0 \rightarrow S_2$	4.23 eV	292.92 (0.0870)	H→L (8.7%), H→L+1 (38.3%), H →L+2 (30.9%), H→L+3 (15.2%), H→L+4 (2.8%)
	$S_0 \rightarrow S_3$	4.26 eV	291.38 (0.0768)	H→L (6.5%), H→L+1 (36.0%), H →L+2 (43.8%), H→L+3 (8.1%), H→L+4 (2.0%)

Table S4 The energy levels and gaps between S_1 and T_1 states for the isolated and coupled units in three polymorphs from the TD-DFT calculation.

		S_1	T_1	$\Delta(S_1\text{-}T_1)$
Crystal (A)	Isolated	4.0805	3.2163	0.8642
	Coupled I	3.9540	3.2130	0.7410
	Coupled II	3.8275	3.1894	0.6381
Crystal (B)	Isolated (B1)	4.0652	3.1788	0.8864
	Isolated (B2)	4.0972	3.2405	0.8567
	Coupled I	4.0528	3.2409	0.8119
	Coupled II	4.0157	3.1798	0.8357
	Coupled III	4.0822	3.1723	0.9099

Crystal (C)	Isolated	4.0371	3.1802	0.8569
	Coupled I	3.9987	3.1405	0.8582
	Coupled II	3.9722	3.1720	0.8002

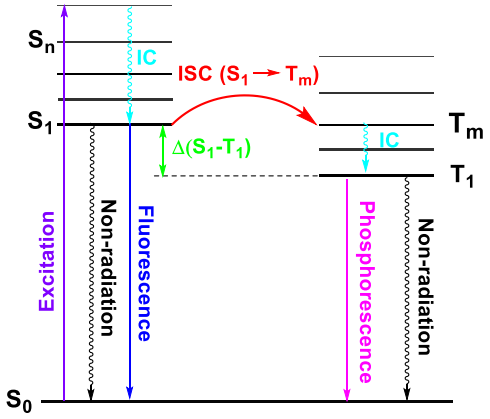

Figure S12 The general diagram for the PL process.

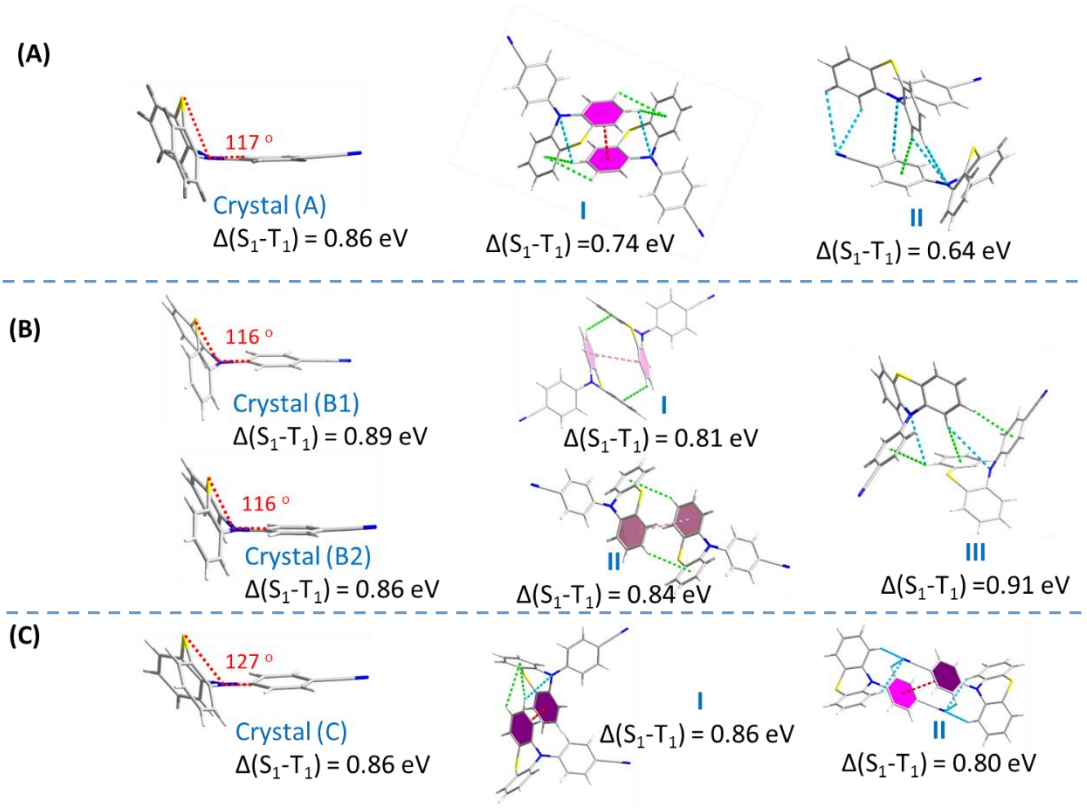

Figure S13 The molecular structures and the respective energy gaps between S_1 and T_1 states for the isolated and coupled units in three polymorphs.

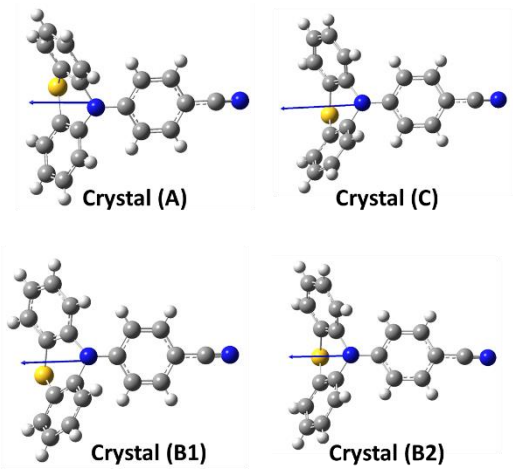

Figure S14 The molecular configurations and the respective transition dipole moments (blue arrows) from S_0 to S_1 states for the three polymorphs.

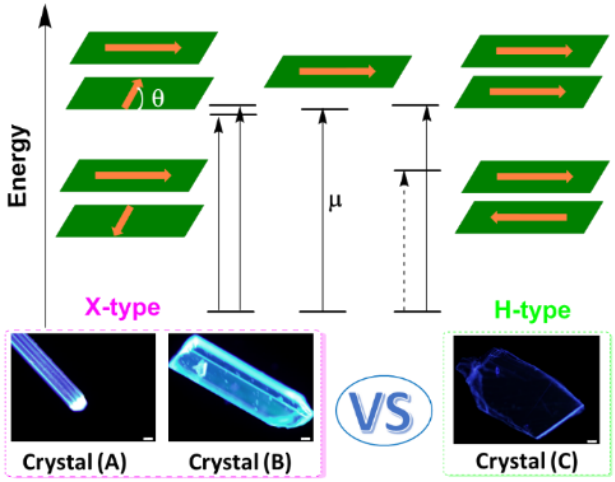

Figure S15 Splitting of the optically allowed transitions of X-type coupled units, isolated molecule and H-type coupled units (upper); the images of the three polymorphs under UV-irradiation taken by optic microscope Leica M123 (down).

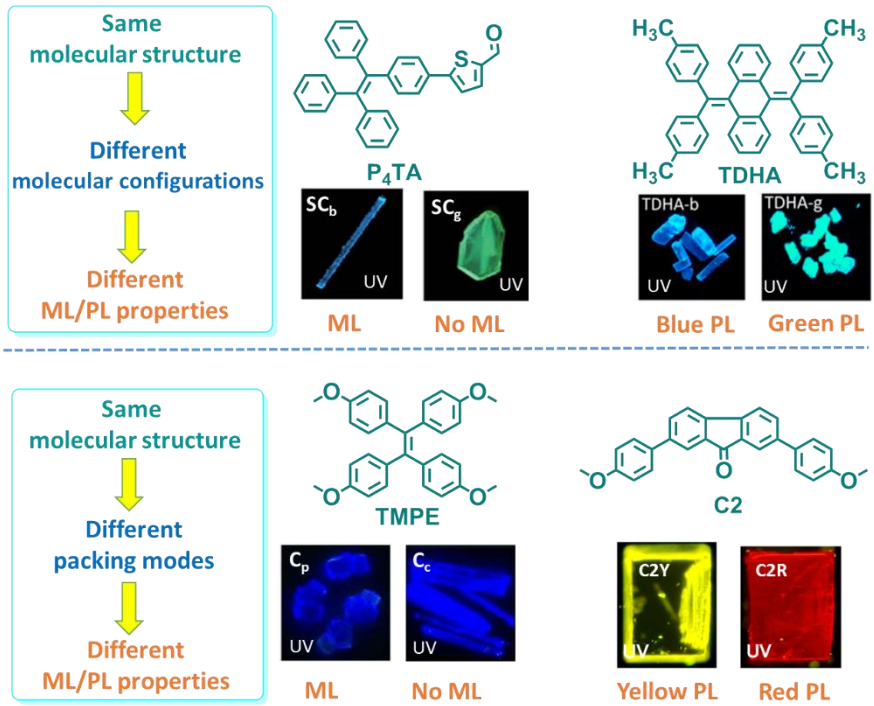

Figure S16 Examples for some polymorphs with diverse emissive properties: For compounds P_4TA and TDHA (upper), the different molecular configurations in polymorphs are mainly responsible for their changed mechanoluminescence (ML)/photoluminescence (PL) properties while for compounds TMPE and C2 (down), the different packing modes in polymorphs should be the main reason.

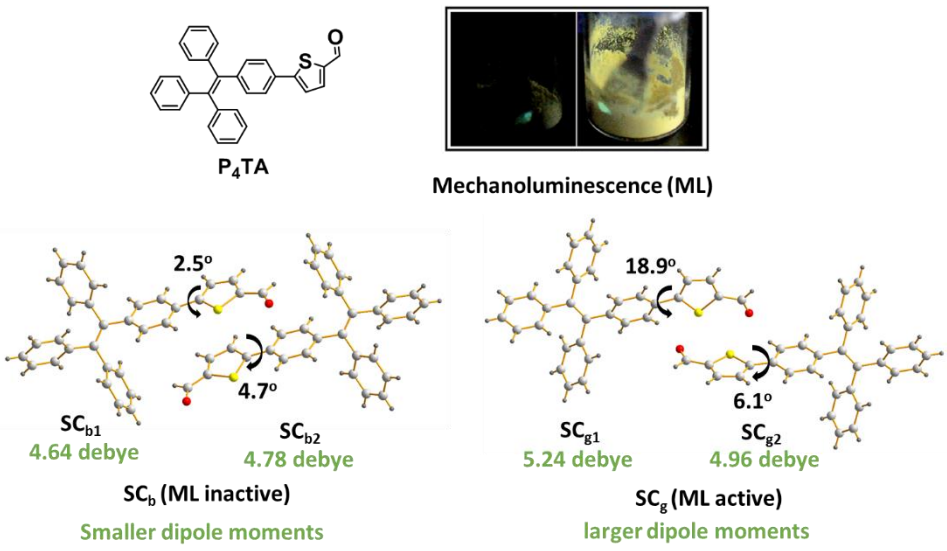

Figure S17 The molecular structure, mechanoluminescence (ML) phenomenon and the crystal analyses of polymorphs for P_4TA—the different molecular configurations with different dipole moments, led to the different ML property.

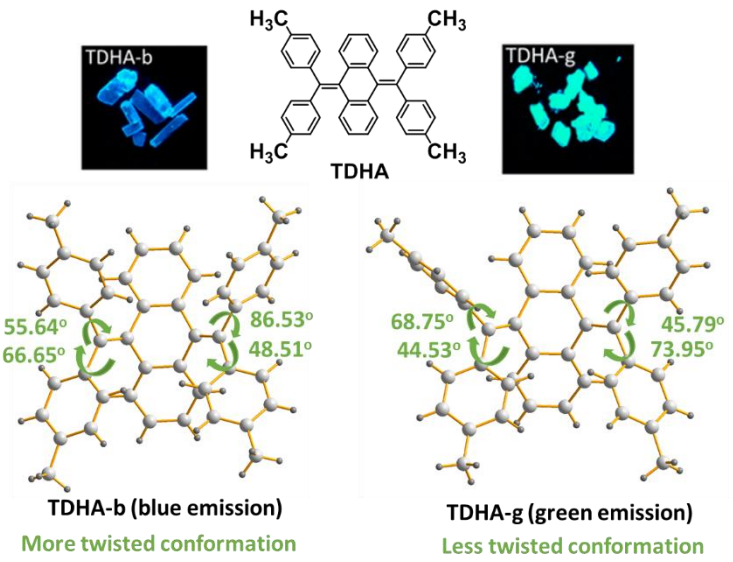

Figure S18 The molecular structure, PL emissive pictures and the crystal analyses of polymorphs for TDHA—the different molecular configurations with different torsion angles, led to the different PL emissions.

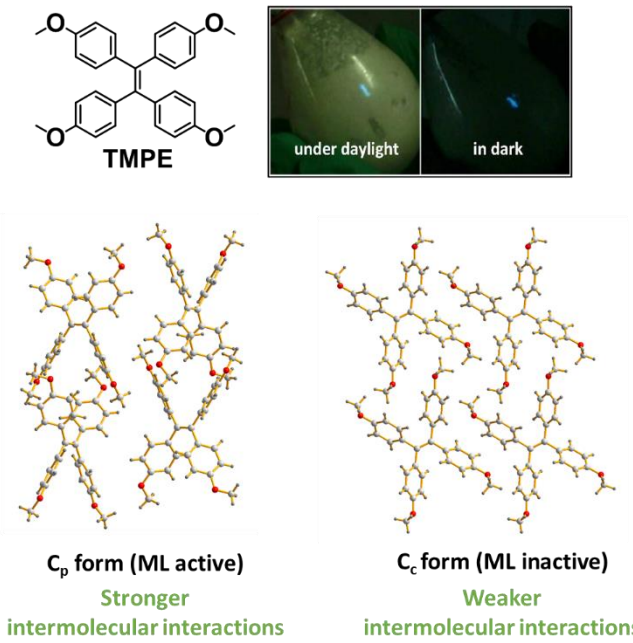

Figure S19 The molecular structure, mechanoluminescence (ML) phenomenon and the crystal analyses of polymorphs for TMPE—the different packing modes with different intermolecular interactions, led to the different ML property.

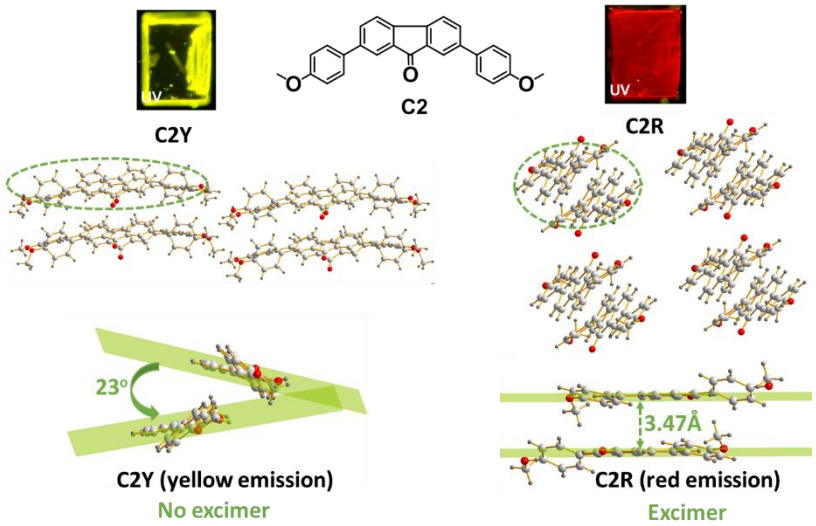

Figure S20 The molecular structure, mechanoluminescence (ML) phenomenon and the crystal analyses of polymorphs for C2—the different packing modes with excimer or not, led to the different PL emissions.